Acta Technica *62* (2017), No. 7A, 311–322

Fault transient location method for distribution network based on generalized sequence model

Zili Yin[1]

Abstract. To improve the accuracy of fault transient location method for distribution network, a fault transient location method for distribution network based on generalized sequence model has been proposed. First of all, the system description and the mathematical model for fault transient location of distribution network are given, and the model can be expressed as a set of differential algebraic equations. Secondly, a generalized sequence model is developed for grid fault location calculation and state space matrix construction, and a dimensionless index for fault transient location of distribution network is put forward. Five different droop location technologies are selected and used for comparative analysis on fault location accuracy. Finally, the effectiveness of the algorithm is verified by analysis of simulation experiment.

Key words. Sequence model, Distribution network, Fault, Transient location.

1. Introduction

The fault diagnosis of power grid plays an important role in fault component recognition, post-fault fast recovery and chain trip avoidance, etc. Artificial intelligence methods, including neural network, pattern matching and Petri net, have been used in power grid fault diagnosis. Bayesian network excels in dealing with the uncertainty of complex problems under incomplete information through the causal reasoning and probabilistic computation, which relatively satisfies the requirements of power grid fault diagnosis. However, in the existing Bayesian network, each node contains all possible states, all of which are difficult to be understood, and have not yet used temporal information, such as protection actions.

The fault location accuracy and load balancing of power grid are two main challenges for power grid. Traditional droop control is proposed for high voltage networks in Literature [3]. For low voltage network, the load distribution is realized with re-

[1]State Grid Fujian Electric power company, Fujian Fuzhou, 350003

verse droop control, virtual inductance and virtual resistance location technologies, but these droop location technologies are disturbed by the low inertia problem. The concept of virtual inertia is presented in Literature [4] to deal with the unnecessary frequency overshoot in transition modes. For the drooping low voltage network is easily affected by load/power generation variations in the system, the study on such islanding network needs to highly focus on fault transient location for distribution network. In Literatures [5-6], the fault location accuracy of islanding network is studied based on the technology of voltage source inverter of generalized dynamic model. The fault location of the power grid could be found by changing the system parameters. When the system parameters change, the qualitative change of the system dynamics is called the bifurcation. Bifurcation analysis has been widely applied to the determination of fault location in power systems [7-8]. In power grid analysis, two kinds of common bifurcations are saddle-node bifurcation and Hopf bifurcation. The saddle-node bifurcation is related to the fault location of the voltage network, and this information can be used for operational planning. When the load parameter variation is more than a certain value, the "vanishes" at the operating point will lead to voltage collapse for the bifurcation. In Literature [10], a continuous algorithm is developed to detect the saddle points in islanding network. When the droop parameter in the islanding network is changed, the Hopf bifurcation is observed. In Literature [11], the impact of change of drooping bifurcation on system fault location accuracy is analyzed. In the existing literature researches, the linear (small-signal) fault location is usually achieved by Hopf bifurcation analysis. However, the Hopf bifurcation could be either subcritical or supercritical. The subcritical Hopf bifurcation leads to non-network fault location limit cycle in the area of grid fault location of parameter space (linearity) which is not accepted [12]. On the other hand, the supercritical bifurcation has the limit cycle of grid fault location in the (linear) non-network fault location region. Therefore, even under the relatively large disturbance, the region of linear grid fault location is also located by the grid fault. It also proves that fault transient location of linear distribution network is enough when the Hopf bifurcation occurs.

This paper has proposed a generalized model to calculate the grid fault location of working point, and then the fault location is determined based on parameter variation. The information required for this model includes generator parameters, line parameters, load parameters and interconnection modes. To guarantee the fault location accuracy of the system, the study on fault location and bifurcation type related to the boundary is critical. In this paper, the dynamics nearby the fault location is studied in detail for value by using this model.

2. System description and mathematical model

2.1. System model

The mathematical model of the power grid can be represented by a set of differential algebraic equations:

$$dx/dt = f\left(X, Y, \mu\right) , \tag{1}$$

$$0 = g\left(X, Y, \mu\right) . \tag{2}$$

Where, X is the state vector; Y is the algebraic vector, and μ is the parameter vector. Generator (inverter, synchronization and asynchronization), load and connection are the main components of the power grid. Specific model definitions are shown in the Literature [3]. In this study, focus on analysis on power transfer from the power source to the power electronics interface and power grid. The inverter control circuit consists of conventional voltage, current and droop controllers. The droop equation in the droop controller provides a reference value for the cascade controller. For each inverter, the model is written in its own reference frame, and then converted to a common reference frame which is arbitrarily selected as the reference frame of the first inverter. The model for connecting lines and loads is written in a public reference frame. The complete power grid model in formulas (1) and (2) is obtained by combining unit models.

2.2. Block diagram method

A generalized model of power grid is given in Fig. 1. In the system, assume that there is/are I inverter(s), B buses, N lines and L loads in total, and they can be represented as separate blocks. This method can be extended to any number of inverters, lines and loads. The parameter vector μ defined in the formula (3) contains all data related to the inverter, line and load; then, the entire power grid can be modeled using matrices (vectors) μ, P_L, P_I and P_N.

$$\mu = \left[P_{\text{inv}}, P_{\text{load}}, P_{\text{line}}\right]^{\text{T}} . \tag{3}$$

Where,

$$P_{\text{inv}} = \left[P_{\text{inv}1}, P_{\text{inv}2}, \cdots, P_{\text{inv}I}\right]^{\text{T}}_{(15I\times 1)} , \tag{4}$$

$$\begin{gathered} P_{\text{inv}k} = [m_{pk}, n_{qk}, \omega_n, V_n, r_c, L_c, r_f, L_f, \\ C_f, F, K_{pv}, K_{iv}, K_{pc}, K_{ic}, \omega_c]^{\text{T}}_{(15I\times 1)} . \end{gathered} \tag{5}$$

Where, m_{pk} is the descent coefficient (rad/Ws) of actual power of inverter; n_{pk} is the droop coefficient (V/VAR) of reactive power of inverter; V_n is the nominal voltage (V); r_c is the coupling inductance resistance (Ω); L_c is the coupling inductance reactance (H); r_f is the filter resistance (Ω); L_f is the filter reactance (H); C_f is the filter capacitance (F); K_{pv}/K_{iv} is the proportional/integral gain of voltage controller;

K_{pc}/K_{ic} is the proportional/integral gain of current controller; ω_c is the ordinary angular velocity, and the subscript k represents the *kth* inverter.

$$P_{\text{load}} = [P_{\text{load}1}, P_{\text{load}2}, \cdots, P_{\text{load}L}]^{\text{T}}_{(3L\times 1)} \ , \tag{6}$$

$$P_{\text{load}k} = [P_{\text{load}k}, P_{\text{load}k}, TYPE_k]^{\text{T}}_{(3L\times 1)} \ . \tag{7}$$

In the formula (7), for constant power load, $TYPE_k = 1$; for RL load, $TYPE_k = 0$

$$P_{\text{line}} = [P_{\text{line}1}, P_{\text{line}2}, \cdots, P_{\text{line}N}]^{\text{T}}_{(2N\times 1)} \ , \tag{8}$$

$$P_{\text{line}k} = [R_{\text{line}k}, L_{\text{line}k}]^{\text{T}}_{(2\times 1)} \ . \tag{9}$$

For the interconnection structure, three matrices P_I, P_N and P_L are defined to determine the positions of inverter, line and load, and respectively shown in the formulas (10-12):

$$P_I = \begin{pmatrix} e_{11} & e_{12} & \cdots & e_{1I} \\ e_{21} & e_{22} & \cdots & e_{2I} \\ \vdots & \vdots & \ddots & \vdots \\ e_{B1} & e_{B2} & \cdots & e_{BI} \end{pmatrix} . \tag{10}$$

In the formula, the node is represented in the longitudinal direction, while the inverter in the horizontal direction. If the node i has the *jth* inverter, $e_{ij} = 1$; otherwise, $e_{ij} = 0$

$$P_N = \begin{pmatrix} e_{11} & e_{12} & \cdots & e_{1N} \\ e_{21} & e_{22} & \cdots & e_{2N} \\ \vdots & \vdots & \ddots & \vdots \\ e_{B1} & e_{B2} & \cdots & e_{BN} \end{pmatrix} . \tag{11}$$

In the formula, the node is represented in the longitudinal direction, while the line in the horizontal direction. If the current in line j enters the node i, $e_{ij} = +1$, and if the current in line j leaves the node i, $e_{ij} = -1$; otherwise, $e_{ij} = 0$

$$P_L = \begin{pmatrix} e_{11} & e_{12} & \cdots & e_{1L} \\ e_{21} & e_{22} & \cdots & e_{2L} \\ \vdots & \vdots & \ddots & \vdots \\ e_{B1} & e_{B2} & \cdots & e_{BL} \end{pmatrix} . \tag{12}$$

In the formula, the node is represented in the longitudinal direction, while the load in the horizontal direction. If the node i has the *jth* node, $e_{ij} = 1$; otherwise, $e_{ij} = 0$.

3. Grid fault location based on generalized sequence model

3.1. Grid fault location calculation and state space matrix

To realize the grid fault location calculation, the problem is solved based on the QR minimization decomposition technique. The process of grid fault location calculation and grid fault location analysis of initial value is given in the algorithm as shown in Fig. 1. The main purpose is to solve the systems (13-14) by using the generalized equations:

$$0 = f\left(\overrightarrow{X}^{e}, \overrightarrow{Y}^{e}_{\mathrm{mg}}, \mu\right) . \tag{13}$$

$$0 = g\left(\overrightarrow{X}^{e}, \overrightarrow{Y}^{e}_{\mathrm{mg}}, \mu\right) . \tag{14}$$

Where, $\overrightarrow{X}^{e}$ is the state vector at the operation point; $\overrightarrow{Y}^{e}_{\mathrm{mg}}$ is the algebraic vector at the operation point, and μ is the parameter vector of change. The state vector contains all state variables of voltage source inverter, line and load. The algebraic vector corresponds to algebraic equation of voltage source inverter. m_p is the parameter to be changed for analyzing the fault location accuracy of the system. The equation set model can be expressed as:

$$F(V) = [DX_{\mathrm{mg}}, G]^{\mathrm{T}} = 0 . \tag{15}$$

Where, V is the set of variables X_{mg} and Y_{mg}; therefore, the system satisfies the stabilization condition. Then, the rectangular matrix can be used for numerical solution:

$$J_F = [\partial F / \partial V] . \tag{16}$$

The partial derivatives of the matrix can be calculated as follows:

$$\frac{\partial F}{\partial V_1} = \frac{F(V_1 + h) - F(V_1)}{h} . \tag{17}$$

In Fig. 1, the stopping threshold TOL is assumed to be 0.001. In this paper, the state space model is directly combined with the grid fault location, and the state space matrix is obtained. The generalized model is linearized, and the state space can be obtained:

$$\frac{d}{dt}\overrightarrow{X}_{\mathrm{mg}} = A\overrightarrow{X}_{\mathrm{mg}} . \tag{18}$$

Where, A is the state matrix of system

3.2. Eigenvalue analysis

Eigenvalue tracking is a common method to determine the small-signal fault location accuracy of power system, oscillation fault location and damping margin. It is feasible to make fault transient location for distribution network with eigenvalue tracking and grid fault location calculation. First of all, when the system is in the

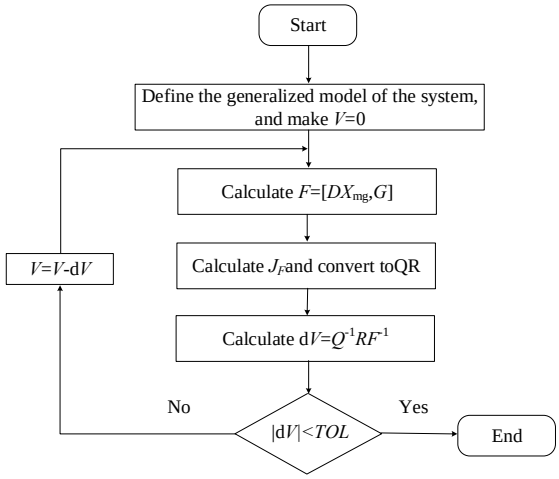

Fig. 1. QR method flow diagram

fault location area of the power grid, detect the eigenvalue of a specific parameter value until the parameter changes to an extent of non-network fault location. If there are n eigenvalues, the index is distributed to the eigenvalue, and an eigenvalue with minimum index is identified to track the possible virtual axis. Assuming that the real part of eigenvalue to be tracked is λ_R, and is the function of parameter μ, it can be represented as:

$$\lambda_R = \psi(\mu) \,. \tag{19}$$

In the location of Hopf bifurcation:

$$\psi(\mu) = 0 \,. \tag{20}$$

Formula (32) can be solved by the Newton Raphson method:

$$\mu_{n+1} = \mu_n - \frac{\psi(\mu)}{d\psi(\mu)/d\mu} = \mu_n - \frac{\lambda_R}{d\lambda_R/d\mu} \,. \tag{21}$$

The paths of the three eigenvalues of parameter μ_i are given in Fig. 2. A point is closest to the virtual axis, but B point is most likely to early contact with the virtual axis than A point, because its $d\lambda_R/d\mu$ more tends towards virtual axis.

It is obvious that in the $\lambda_R - \mu$ plane, the traceability of eigenvalue is determined at the current position in the plane of eigenvalue. Therefore, it is necessary to choose the eigenvalues with relatively large slope close to the virtual axis. The process of eigenvalue tracking is shown in Fig. 4.

In Fig. 3, the tracking process of eigenvalues is accomplished by calculating the given index:

$$I_i = \left| \frac{\lambda_R}{d\lambda_R/d\mu} \right| \,. \tag{22}$$

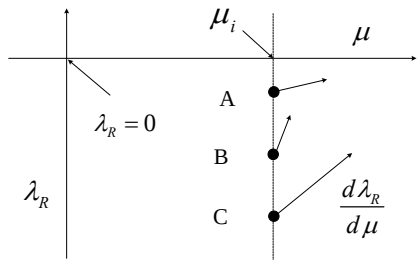

Fig. 2. Feature tracking

Where, I_i is the index of the *ith* eigenvalue. The iterative process is then performed with the selected eigenvalue. At the Hopf bifurcation point, the ideal value of real part of the eigenvalue tracking is zero. The eigenvalue tracking algorithm stops when the absolute value of real part of the eigenvalue tracked is less than the error tolerance.

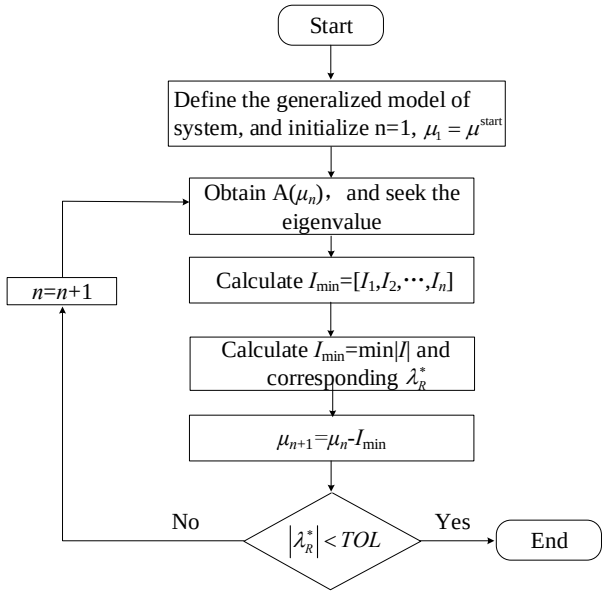

Fig. 3. Tracking process of eigenvalues

4. Experimental analysis

4.1. Simulation conditions introduction

To verify the above analysis results, the IIDG simulation model is built on the PSCAD/EMTDC simulation platform. The parameters of the IIDG model are shown as follows: including the rated capacity of 10.0 MVA, the rated voltage of

10.5 kV, the filter inductance of 8 and the filter inductance equivalent resistance of 0.5mΩ.

4.2. Symmetrical voltage drop

The simulation verification is conducted for IIDG fault current characteristics with the fault condition where three-phase voltage of power grid symmetrically drops to 40% for example. In Fig. 4, components of d and q axle of IIDG output current in rated condition prior to fault and corresponding values given are presented. Waveforms of A-phase fault current i_a, amplitude i_{am} and phase difference P_{ui} between current and voltage are shown in Fig. 5.

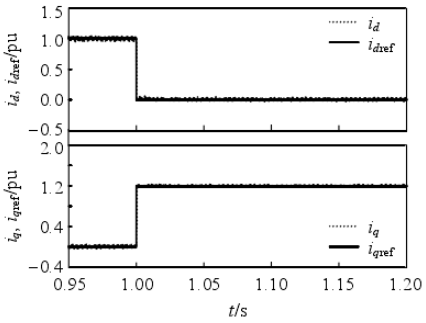

Fig. 4. Fault current features of IIDG

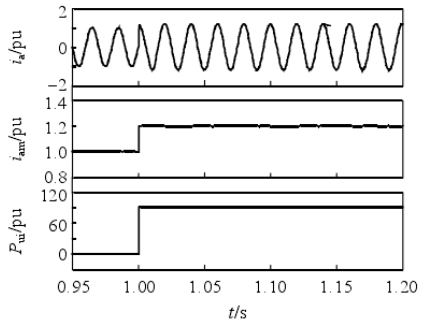

Fig. 5. A-phase fault current of IIDG

After the drop, the three-phase voltage of power grid remains symmetrical, and the amplitude drops from 1.0 pu to 0.4 pu. According to the low voltage ride-through control strategy proposed in this paper, the post-fault reactive current order is 1.2 pu, and to prevent from converter damage for over-current, and active current order is reduced to 0, which is shown in Fig. 5. It can be seen that the output current of IIDG can rapidly track the order within 1ms. From Fig. 6, we can see that for IIDG is in the rated operation before the fault, the amplitude change of fault current fed out is relatively small, even although the amplitude of voltage drop is large. After the voltage drop, to provide reactive power support to the grid, the

IIDG only outputs the reactive current, which leads to a phase difference between A-phase current and voltage from 0o to 900o.

Fig. 6 shows the components of d and q axle of IIDG output current when the idle running before fault and the network voltage symmetrically drops to 40% and corresponding values given. Fig. 7 presents the waveforms of A-phase fault current i_a and its amplitude i_{am}. For the idle running of IIDCT before fault, the output current is 0, and the phase is meaningless; therefore, the phase waveform of the IIDCT output current is not given here.

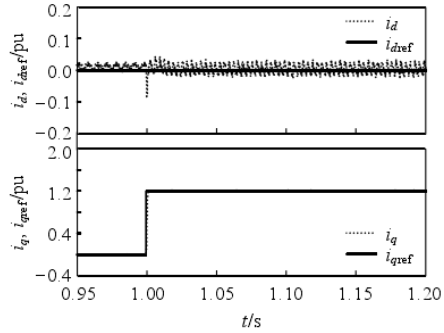

Fig. 6. Components of d and q axle of fault current of IIDG under idle running before fault

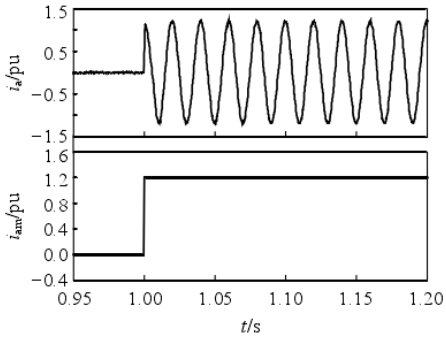

Fig. 7. A-phased fault current of IIDG under idle running before fault

As shown in Fig. 6, after the network voltage drop, the reactive current order is 1.2 pu and the active current order is still 0, and the output current of IIDG could quickly track the order. From Fig. 7, it can be seen that the amplitude of fault current fed from IIDG changes from 0 to 1.2pu for the IIDG is in the idle running before the fault.

5. Conclusion

In this paper, a generalized sequence mode model has been developed for grid fault location calculation and state space matrix construction, and a dimensionless index for fault transient location in distribution network is put forward for analysis on problem of fault location accuracy on the islanding network model. Finally, with IEEE 33 bus system for example, the problem of fault location on the islanding network is analyzed, and it shows that the system could determine the working point through QR algorithm when the sag is in the positive boundary from the working point of grid fault location, even under the situation of large disturbance. Especially, when the system is outside the boundary, the system will tend to the limit cycle of grid fault location.

References

[1] Y. Y. Zhang, Q. Li, W. J. Welsh, P. V. Moghe, and K. E. Uhrich: *Micellar and Structural Stability of Nanoscale Amphiphilic Polymers: Implications for Anti-atherosclerotic Bioactivity*, Biomaterials, *84* (2016), 230–240.

[2] J. W. Chan, Y. Y. Zhang, and K. E. Uhrich: *Amphiphilic Macromolecule Self-Assembled Monolayers Suppress Smooth Muscle Cell Proliferation*, Bioconjugate Chemistry, *26* (2015), No. 7, 1359–1369.

[3] Y. Y. Zhang, E. Mintzer, and K. E. Uhrich: *Synthesis and Characterization of PEGylated Bolaamphiphiles with Enhanced Retention in Liposomes*, Journal of Colloid and Interface Science, *482* (2016), 19–26.

[4] Y. Y. Zhang, A. Algburi, N. Wang, V. Kholodovych, D. O. Oh, M. Chikindas, and K. E. Uhrich: *Self-assembled Cationic Amphiphiles as Antimicrobial Peptides Mimics: Role of Hydrophobicity, Linkage Type, and Assembly State*, Nanomedicine: Nanotechnology, Biology and Medicine, *13* (2017), No. 2, 343–352.

[5] Y. Liao: *Generalized fault-location methods for overhead electric distribution systems*[J]. IEEE Transactions on Power Delivery, *26* (2011), No. refeq1, 53–64.

[6] V. Venkatasubramanian, R. Rengaswamy, S. N. Kavuri, et al.: *A review of process fault detection and diagnosis: Part III: Process history based methods*[J]. Computers & chemical engineering, *27* (2003), No. 3, 327–346.

[7] R. H. Salim, K. R. C. de Oliveira, A. D. Filomena, et al.: *Hybrid fault diagnosis scheme implementation for power distribution systems automation*[J]. IEEE Transactions on Power Delivery, *23* (2008), No. 4, 1846–1856.

[8] Z. Su, Y. Lu: *A new wavelet packet analysis based method to detect faulty line for single phase to ground fault occurred in distribution network with small current neutral grounding*[J]. Power System Technology, *12* (2004), 30–33.

[9] M. J. B. Reddy, D. K. Mohanta: *Performance evaluation of an adaptive-network-based fuzzy inference system approach for location of faults on transmission lines using Monte Carlo simulation*[J]. IEEE Transactions on Fuzzy Systems, *16* (2008), No. 4, 909-919.

[10] O. Chaari, P. Bastard, M. Meunier: *Prony's method: an efficient tool for the analysis of earth fault currents in Petersen-coil-protected networks*[J]. IEEE Transactions on Power Delivery, *10* (1995), No. 3, 1234–1241.

[11] E. E. Ngu, K. Ramar:*A combined impedance and traveling wave based fault location method for multi-terminal transmission lines*[J]. International Journal of Electrical Power & Energy Systems, *33* (2011), No. 10, 1767–1775.

[12] Z. Gao, C. Cecati, S. X. Ding: *A survey of fault diagnosis and fault-tolerant*

techniques—Part I: Fault diagnosis with model-based and signal-based approaches[J]. IEEE Transactions on Industrial Electronics, *62* (2015), No. 6, 3757-3767.

[13] M. Jamil, A. Kalam, A. Q. Ansari, et al.: *Generalized neural network and wavelet transform based approach for fault location estimation of a transmission line*[J]. Applied Soft Computing, *19* (2014), 322–332.

[14] M. Majidi, M. Etezadi-Amoli, M. S. Fadali: *A novel method for single and simultaneous fault location in distribution networks*[J]. IEEE Transactions on Power Systems, *30* (2015), No. 6, 3368–3376.

[15] A. Dasgupta, S. Nath, A. Das: *Transmission line fault classification and location using wavelet entropy and neural network*[J]. Electric Power Components and Systems, *40* (2012), No. 15, 1676–1689.

[16] L. S. Martins, J. F. Martins, V. F. Pires, et al.: *The application of neural networks and Clarke-Concordia transformation in fault location on distribution power systems*[C]//Transmission and Distribution Conference and Exhibition 2002: Asia Pacific. IEEE/PES. IEEE, *3* (2002), 2091–2095.

Received May 7, 2017